Directed Acoustic Shearography

Russell M. Kurtz*
RAN Science & Technology, LLC, 2101 Via Rivera, Palos Verdes Estates, CA 90274

ABSTRACT

Modern vehicles use modern materials, including multiple metallic layers, composites, and ceramics. This has led to significant improvements in quality, reliability, and lifetime, at the cost of significantly increased complexity. It is particularly difficult to test these modern materials for buried defects such as internal corrosion, glue/weld failures, and disbonds, yet these defects can lead to damage and even failure of the part. As one tool in the array of nondestructive evaluation (NDE) technologies, we report on Directed Acoustic Shearography (DAS), which combines the sensitivity of shearography with the speed of ultrasonic imaging, and adds improved depth resolution. We show that DAS is particularly useful in detecting buried defects in modern materials, how it lends itself to automation, and present early tests of DAS detecting buried defects as small as 1/32 inch in a multilayer aluminum structure.

Keywords: Nondestructive Evaluation, NDE, Acoustic, Shearography, Phased Array, Directed Acoustic Shearography

1. INTRODUCTION

Subsurface defects are a major concern in the transportation industry. During the past decade, more than 1,650 aircraft accidents have been reported,[1] a large percentage of them caused by corrosion or other buried damage. A number of automobile recalls have also been caused by buried defects. When these defects or damage occur in modern materials, made up of several layers in a composite structure, detection can be difficult and expensive. In some automobiles, for example, it is possible to partially disassemble the area in which corrosion is suspected, check it visually, and reassemble it in a short time. More recent vehicles, and aircraft in particular, take much more time and effort to disassemble; in many structures, such disassembly itself causes damage. Modern composites often cannot be disassembled at all. It is, therefore, critical to develop a nondestructive evaluation (NDE) technology that can find these buried defects, corrosion, or damage spots rapidly, accurately, and efficiently.

Most existing NDE technologies, such as holography,[2] eddy current,[3] and thermography,[4] are better at finding surface cracks than buried defects. Other, more exotic techniques, such as x-ray imaging,[5] THz transmission,[6] and computed tomography,[7] require access to both sides of a piece; this may not be possible, for example, in aircraft wings, assembled automobiles, or ships. Shearography has the capability of detecting buried defects,[8] and has been demonstrated successfully when the shearographic stress source was thermal.[9] Thermal diffusion, however, is very slow; in a typical automobile part, 0.3 in. thick, the time required to test one "spot" (typically ~1 cm^2) using thermal shearography is ~3 s.

Using an acoustic signal as the shearographic stress, however, is fast. In that same 0.3-in. automobile part, the acoustic stress propagates to the deepest area of interest in <3 μs (assuming typical materials, such as aluminum, titanium, or carbon fiber composites). This factor of 10^6 increase in stress propagation enables much shorter measurement times, limited by the speed of the electronics and imaging rather than the stress propagation. The rapid propagation also enables measurement of several samples in a short time, improving the resolution and signal-to-noise ratio (SNR) of the technique. Shearography using an acoustic stress source is the basis of Directed Acoustic Shearography.

2. THEORY

Digital Acoustic Shearography (DAS) is an application of shearography, using a directed acoustic beam as a stress source. The background and specific theory of DAS is developed in this section.

2.1 Shearography

Shearography can be considered as differential surface metrology. A reference scan of the surface is taken in the absence of stress. Stress is then applied to the material. The applied stress interacts with any voids, cracks, or defects in the material to produce a surface strain. Another scan—the stress scan—is performed under the stress conditions. The

* Russell.Kurtz@ranscitech.com; phone 1 310 592-7901; fax 1 413 208-7269; www.ranscitech.com

Photonics in the Transportation Industry: Auto to Aerospace III, edited by
Alex A. Kazemi, Bernard C. Kress, Eric Y. Chan, Proc. of SPIE Vol. 7675, 76750B

stress scan is subtracted from the reference scan (or *vice versa*), resulting in a shear scan that highlights the surface strain (Fig. 1).

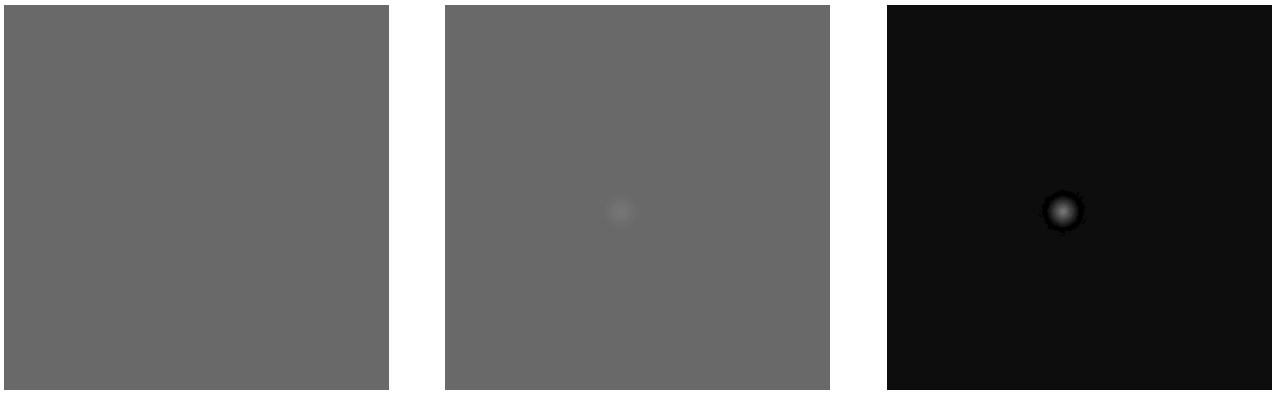

(a) (b) (c)

Fig. 1. The difference between a reference scan (a) and a stress scan (b) produces a shear scan (c), which highlights changes in the surface strain.

If we define the normal to the surface as the *z*-direction, and match this to the measurement direction, we can write the surface function, measured by the reference scan, as

$$s_{ref} = z_1\left(x, y\right). \tag{1}$$

The stress scan will then measure

$$s_{stress} = z_2\left(x, y\right) = z_1\left(x, y\right) - \Delta z\left(x, y\right). \tag{2}$$

If the depth of the original defect is known, or can be calculated, the surface strain can be measured:

$$\varepsilon\left(x, y\right) = \Delta z\left(x, y\right) \Big/ z_{def} \equiv \left(s_{ref} - s_{stress}\right) \Big/ z_{def}\ , \tag{3}$$

where z_{def} is the depth of the defect. The unbalanced, applied stress, as a function of measurable data, known parameters, and defect depth, can be calculated (in isotropic media, such as most metals) as

$$\sigma\left(x, y, z_{def}\right) = E\left(s_{ref} - s_{stress}\right) \Big/ z_{def}\ , \tag{4}$$

where E is the Young modulus of the material. (For non-isotropic materials, such as many composites, the derivation is similar, but the full stress, strain, and Young modulus tensors must be used.) Eq. (4) demonstrates that the induced stress can be determined from a simple shearographic measurement.

A number of stress methods can be used for shearography. One common method is to apply heat, through (for example) an external heating laser. This can be slow, since the heat diffusion rate is low; for example, in aluminum it is 0.96 cm^2/s, in carbon steel it is 0.12 cm^2/s, and in titanium it is 0.093 cm^2/s. For these three common metals, it takes between 3 and 60 s for thermal equilibrium to be reached at the 0.3-in. depth of our model automobile part.

Other stress methods include tapping, pressure, and acoustic signal. Of these, the acoustic (or ultrasonic) signal is the easiest to control. In addition, the speed of sound in metals is so high (typically ~5000 m/s) that the stress propagates through the model depth virtually instantly (1.5 μs). A typical spherical acoustic wave, however, is not a good choice for stress application, since its intensity decreases at least as fast as the depth squared.

2.2 Directed Acoustic Shearography

It is clear, then, that an acoustic signal could be a good source of stress, if it could be collimated (or focused) and directed. Fortunately, this can be accomplished with a phased array acoustic transducer (PA). A standard equation of wave propagation, the Huygens-Fresnel principle, states that the amplitude U of a wave signal at location (x, y, z) is the sum of individual spherical waves that were, effectively, generated at locations (x, y, 0), where the wave propagates

along z. For mathematical convenience, we rename $x \rightarrow \xi$ and $y \rightarrow \eta$ at the plane $z = 0$. If we assume that the acoustic wave is continuous at that plane, the sum becomes an integral,

$$U(x,y,z) = \frac{e^{i\vec{k}\bullet\vec{r}}}{i\vec{k}\bullet\vec{r}} \int_{-\infty}^{\infty}\int_{-\infty}^{\infty} U(\xi,\eta) e^{i\vec{k}\bullet\vec{r}}\, d\xi\, d\eta\,, \tag{5}$$

where $\vec{r} \equiv x\hat{x} + y\hat{y} + z\hat{z}$ and $\vec{k}$ is the propagation vector, satisfying

$$\left|\vec{k}\right| = 2\pi/\lambda\,. \tag{6}$$

Defining the two-dimensional Fourier transform

$$F(\omega_x,\omega_y) = \Im\left[U(\xi,\eta)\right] \equiv \frac{1}{2\pi}\int_{-\infty}^{\infty}\int_{-\infty}^{\infty} U(\xi,\eta) e^{i\left(\xi\omega_x + \eta\omega_y\right)}\, d\xi\, d\eta\,, \tag{7}$$

in the far field we can combine eqs. (5-7) to write

$$U(x,y,z) = \frac{e^{i2\pi z/\lambda}}{i2\pi z/\lambda} \exp\left[i\frac{\pi}{\lambda z}\left(x^2 + y^2\right)\right] F(\omega_x,\omega_y), \tag{8}$$

where the Fourier frequencies are calculated at $\omega_x = x/2\pi\lambda z$ and $\omega_y = y/2\pi\lambda z$. In other words, the far-field amplitude is proportional to the Fourier transform of the amplitude at $z = 0$. More importantly, the acoustic intensity can be calculated from eq. (8) as

$$J(x,y,z) = \beta\frac{\lambda^2}{z^2}\left|F\left(\frac{x}{2\pi\lambda z}, \frac{y}{2\pi\lambda z}\right)\right|^2, \tag{9}$$

where β is a proportionality constant that depends on the material and acoustic polarization (transverse or longitudinal). Thus, the intensity at any point can be determined by selection of the amplitude at the plane defined as $z = 0$.

A PA can be used to define $U(\xi, \eta, 0)$. In general, the PA is a 2D array of transducers whose relative phase and intensity can be controlled. (We assume that they all operate at the same frequency, thus generate acoustic signals at the same wavelength; if the array is 3D, this appears as a change in the modeled 2D phase.) It is possible, then, to focus the signal down to a narrow spot, or to create a collimated beam of acoustic intensity. As a general rule, the collimated beam is desired for DAS; it is a truly *directed* acoustic signal.

2.3 Advantages of DAS

We determined in Section 2.1 that an acoustic signal can be very useful as a stress source. If the signal is simply a spherical wave, however, propagation of a 1-W signal across the 0.3-in. model thickness results in acoustic intensity of 0.274 W/cm^2, while the same signal, if collimated into an acoustic beam whose diameter is 0.1 in., produces an acoustic intensity at the same depth of 19.7 W/cm^2. This increase in acoustic intensity increases induced stress at a defect by the same factor.

More importantly, the collimated beam improves defect resolution. In most shearographic measurement, the shear scan is correlated to the induced stress point-by-point. DAS takes a different approach, using the acoustic beam to increase system resolution. When the beam is injected into a material, only the locations in which the beam intersects a defect will result in induced stress; thus, only in this case will the surface profile change. By adjusting the relative phasing of the PA, the beam can be scanned in angle; by moving the PA along the surface, the beam can be scanned in location (Fig. 2).

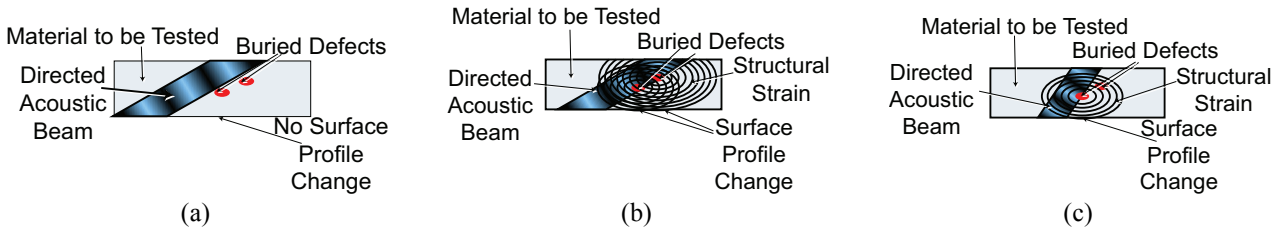

Fig. 2. If the directed acoustic beam does not strike any defects (a), there is no surface profile change. If it intersects two at different depths (b), there is a complex surface profile change. Rescanning at a different angle (c) enables the beam to apply stress to a single defect at a time, resulting in a spherical surface profile change.

If the defect encountered by the acoustic beam is smaller than the beam, the resulting surface profile change is nearly spherical. If the beam encounters more than on defect (Fig. 2(b)), the surface deflection is a sum of near-spherical strain variations; it is possible to calculate the anticipated surface change from the defects. It is easier, however, to scan the beam in both position and angle. For accurate determination of defect depth, a minimum of four scans must be performed at different angles; the exact number depends on the thickness of the material. If the beam diameter is d, the length of the material is x_0, and its width is y_0, we can define $M \equiv 2x_0/d$ and $N \equiv 2y_0/d$; then the minimum number of scans needed to unambiguously detect buried defects is $4 \times M \times N$.

3. MODELING AND EXPERIMENT

To test the DAS concept, we fabricated test coupons. These were rectangular pieces of aluminum, mechanically polished on one side (to ~120 R_a, not mirror-like), with 5/16-in. diameter holes drilled on 1-in. centers. This made it possible to mount the coupons on a block threaded for 1/4-20 screws (Fig. 3). The buried defect to be discovered was a small nick on the back side, made with a 1/32-in. drill.

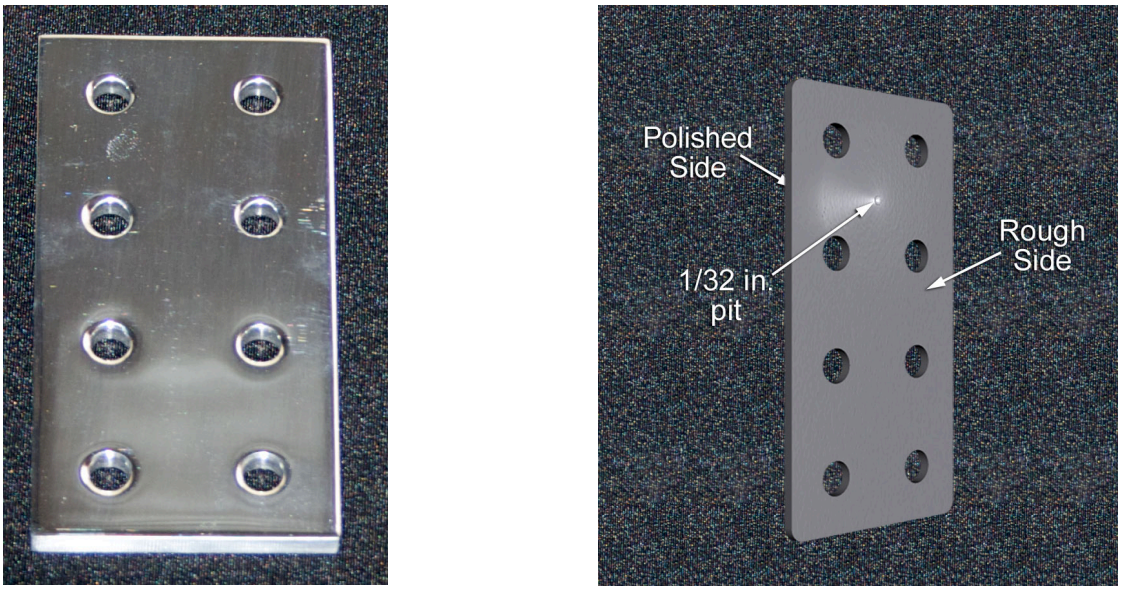

Fig. 3. The test coupons were 2×4 inches, drilled on 1-inch centers. One side (a) was polished, the other (b) was rough. The rough side had a small defect made by a 1/32-inch drill.

3.1 Finite Element Modeling

We assumed the test coupons would be mounted firmly by the 1/4-20 bolts. This provided boundary conditions for modeling the surface deflection induced by the acoustic stress, using the finite element method. We found that a 0.1-in. diameter collimated beam, whose total acoustic power was 125 mW, would induce a surface deflection of >7.5 µm if it encountered a 1/32-in. defect on the back of a 0.1-in. thick plate of Al (Fig. 4).

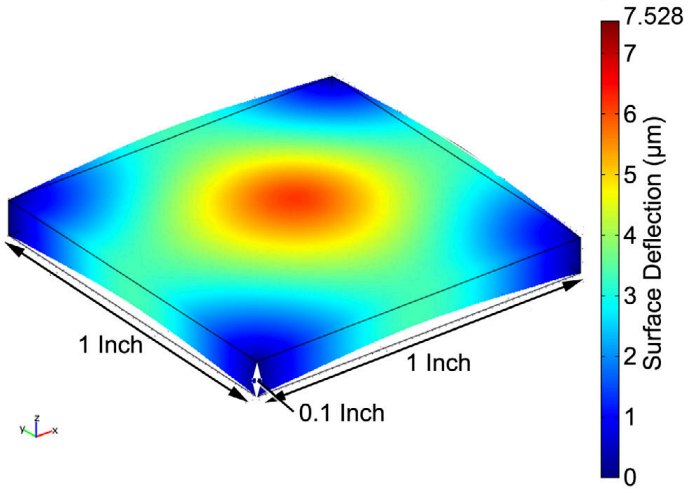

Fig. 4. Finite element analysis of a 0.1-inch aluminum plate with a 0.03-inch diameter defect on the back, using a 0.1-inch diameter collimated, 125-mW acoustic beam indicates that the surface profile expands 7.5 µm at the center (and is held in place by bolts at the corners).

The surface deflection of 7.5 µm at the center is equivalent to a surface curvature change from flat to convex, with a curvature radius of 14.5 m. Although not a large curvature—it is difficult, for example, to purchase lenses whose radius is this large—this curvature is easy to detect with shearography. The curvature induced by the modeled 125-mW beam striking a defect on the back of test coupons is shown as a function of coupon thickness in Fig. 5. We have estimated that our prototype metrology system can detect curvature whose radius is <300 m. Finite element modeling also indicated that the radius of curvature was approximately inversely related to the acoustic power; greater depths can be probed if more power is used.

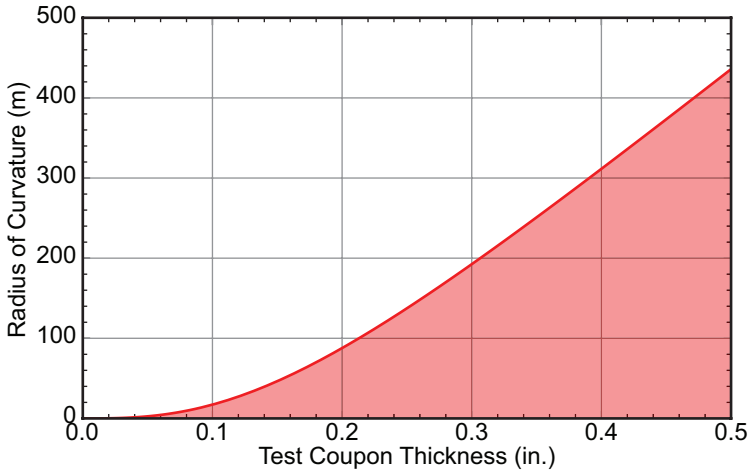

Fig. 5. While a 0.1-inch thick piece of aluminum results in 14.5-m radius of curvature, the modeled 0.3-inch automotive part would demonstrate nearly 200 m radius.

3.2 Experiment

To test the DAS concept, and our finite element modeling, we performed an experiment on a test coupon whose thickness was 0.1 in. Instead of a PA, we used a piezoelectric transducer mounted about 1.2 in. from the in-plane location of the defect (see Fig. 6). The transducer was run at a relatively low frequency, 20 kHz, due to limitations of the equipment (an ideal frequency would be closer to 500 kHz). We tested the system at two voltage levels, 0-9 V and 0-30 V to the piezo stack, which correspond to 450 mW and 1.5 W acoustic power. Propagating the acoustic signal through the aluminum plate, we find that the acoustic intensities are equivalent to 30 mW and 100 mW in our modeled

0.1-in. diameter beam; the propagated acoustic intensity at the lower voltage was 590 mW/cm^2 and the higher voltage resulted in propagated acoustic intensity 2.0 W/cm^2.

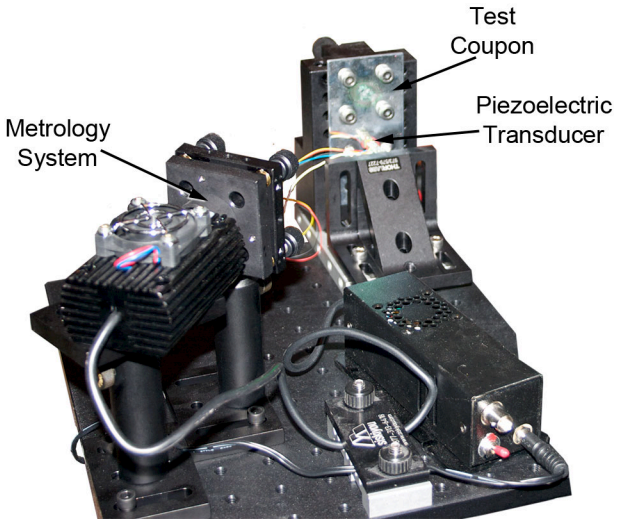

Fig. 6. The DAS test setup used a metrology system to measure surface profile of the test coupon and a piezoelectric transducer to generate acoustic stress.

The DAS test demonstrated the advantages of differential measurement. With the metrology system viewing the surface at ~45°, looking only at the square within the edges of the bolts, it was not easy to see differences among the profiles with or without stress (Fig. 7).

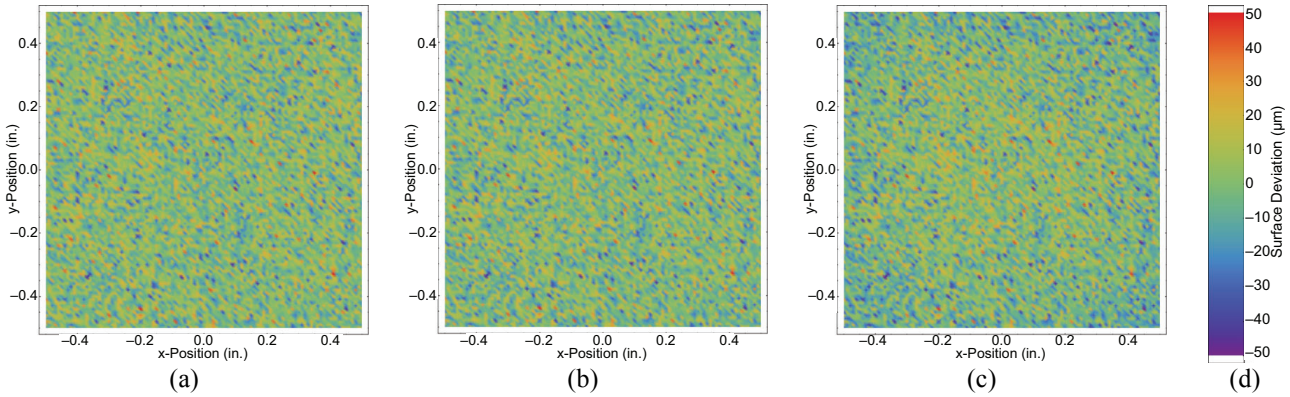

Fig. 7. Scrutinization of the surface profiles shows a slight difference between unstressed condition (a), low power (b), and high power (c) acoustic stress. The scale for all three is -50 µm to 50 µm (d).

Surface metrology showed the roughness of the test coupon, even though it looked polished. These measurements indicate RMS surface roughness of ~10 µm. If we study the three profiles, there appears to be little difference between Fig. 7(a) and Fig. 7(b), although Fig. 7(c) indicates slightly lower profile in the corners. Taking the difference of the calculated surface profiles, however, shows significant curvature in the stressed cases (Fig. 8). The curvature under low acoustic stress is calculated to have a radius of 67 m, while that under high acoustic stress has a calculated radius of 19 m. This corresponds to 2.9 µm and 10 µm maximum surface deflection, respectively. The negative values of the difference are artifacts of the calculation and noise-reduction software.

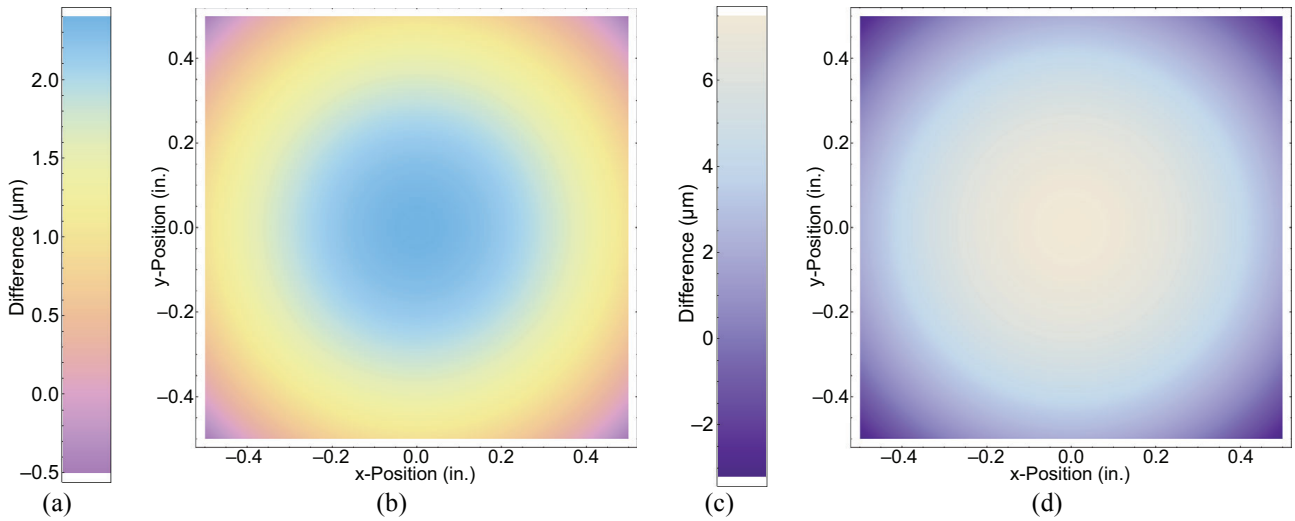

Fig. 8. Under low acoustic stress, the deflection above the defect is still easily detectable in the shear image. The net deflection increase is 2.9 µm with 9 V driving the piezoelectric transducer (b; scale is a), and 10 µm with 30 V applied to the piezoelectric transducer (d; scale is c). The driving voltage was a 20 kHz sine wave and the stated voltages are peak-to-peak, since the piezo would not accept negative drive voltage.

4. SUMMARY, CONCLUSIONS, AND FUTURE WORK

The concept of Directed Acoustic Shearography has been proven. Using high-sensitivity metrology, the surface profile of a test coupon (0.1-in. thick Al, mechanically polished to ~10 µm RMS surface roughness, with a specified defect of size 1/32 in. on the back) was scanned under conditions of no stress, 590 mW/cm^2 acoustic stress, and 2.0 W/cm^2 acoustic stress. Due to the surface roughness, it was difficult to see any change in the surface profile. The unstressed scan values were then subtracted from the surface profile values under stress.

The theory of DAS was developed, using a phased array acoustic transducer to generate a steerable, collimated acoustic beam. By scanning the transducer in angle and translating it along the surface of the material under test, subsurface defects can be located in three dimensions with resolution better than the diameter of the acoustic beam. In the absence of a PA or scanning system, the DAS principle was proven by detecting the defect under acoustic stress produced by a single piezoelectric transducer, operating at 20 kHz, positioned 1.2 in. away from the defect. Images of the surface profile differences demonstrated that the stress induces near-spherical deformation of the test coupon surface, and this deformation is easily measured in the difference image because the surface roughness has been subtracted with the reference scan.

While the principle of DAS has been demonstrated, it is not yet a fieldable measurement system. Future work includes calibrating the difference images, studying the effects of more than one defect and off-center defects, implementing a collimated, directed acoustic beam, and scanning in both angle and position.

5. ACKNOWLEDGEMENTS

We gratefully acknowledge the support of the U.S. Air Force under contract FA8501-09-P-0111.

6. REFERENCES

[1] "Aircraft Crashes Record Office," http://www.baaa-acro.com/ (2010).
[2] Fein, H., "Holographic Analysis of the Structural and Operational Dynamics of an Advanced Graphite-Epoxy Composite Flight Control Structure," Proc SPIE 3397, pp. 179-188 (1998).
[3] Sicard, R., Serhan, S., and Grimard, N., "Detection and Imaging of Corrosion and Cracks in Multi-Layered Aluminum Aircraft Structures Using Pulsed Eddy Currents," (2008).
[4] Safai, M., Georgeson, G., and Meredith, K., "Thermographic Non-Destructive Testing Using Inductive Thermal Excitation," Proc SPIE 6934, pp. 69340M-69349 (2008).

[5] Abou-Khousa, M.A., Ryley, A., Kharkovsky, S., Zoughi, R., Daniels, D., Kreitinger, N., and Steffes, G., "Comparison of X-Ray, Millimeter Wave, Shearography and through-Transmission Ultrasonic Methods for Inspection of Honeycomb Composites," Proc AIP 894, pp. 999-1006 (2007).
[6] Anastasi, R.F., Madaras, E.I., Seebo, J.P., Smith, S.W., Lomness, J.K., Hintze, P.E., Kammerer, C.C., Winfree, W.P., and Russell, R.W., "Terahertz NDE Application for Corrosion Detection and Evaluation under Shuttle Tiles," Proc SPIE 6531, pp. 65310W-65316 (2007).
[7] Martz, H.E., Schneberk, D.J., and Roberson, G.P., "Three-Dimensional Nonintrusive Imaging of Obscured Objects by X-Ray and Gamma-Ray Computed Tomography," Proc SPIE 1942, p. 236 (1993).
[8] Newman, J.W. and Butera, M., "Laser Shearography Technology," (2008).
[9] Kurtz, R.M., Piliavin, M.A., Pradhan, R.D., Tun, N., Aye, T.M., Savant, G.D., and Hergert, S., "Reflection Shearography for Non-Destructive Evaluation," Proc Proc. SPIE 5422, pp. 532-540 (2004).